Available online at www.sciencedirect.com
SCIENCE DIRECT
Polymer 47 (2006) 3171–3185
polymer
www.elsevier.com/locate/polymer

# Morphological alteration and strength of polyamide 6 subjected to high plane–strain compression

Xiaoyu Chen [a,1], Andrzej Galeski [a,*], Goerg H. Michler [b]

[a] *Centre of Molecular and Macromolecular Studies, Polish Academy of Sciences, 90-363 Lodz, Poland*
[b] *Institute of Materials Science, Martin Luther University Halle-Wittenberg, D-06099 Halle/Saale, Germany*

Received 23 November 2005; received in revised form 17 February 2006; accepted 21 February 2006
Available online 23 March 2006

**Abstract**

The present study attempts to find out the similarity and dissimilarity in structure and mechanical properties of PA6 deformed by channel die compression and by a new method combining the compression and rolling and which is known as rolling with side constraints. The resulting materials were characterized by texture investigation by WAXD and SAXS while mechanical properties by tensile tests and DMTA. The fractured surfaces of rolled samples at high deformation ratio was visualized by using SEM. The present study indicates that the crystalline texture and lamellar structure of PA6 samples after the deformation by the two methods are similar at the corresponding strains, some differences develop at a hardening stage at which the time allowed for creep under load plays an important role. Above the compression ratio of 1.8 an intense shear banding occurs at $\pm 45°$. With further deformation to compression ratio of 4.0 the shear band planes are tilted 20–26° from the flow direction only. In association with the appearance of shear bands a fraction of γ-form crystals is generated which are oriented with macromolecular chain axes along shear planes and in the direction of shear. Those γ-crystals are misaligned with α-crystals that are deformed and oriented along the flow direction. The bifurcation of orientation of α- and γ-crystals is a reason of a unique fracture behavior of highly oriented samples: fracture occurs along shear planes with γ-crystals and fracture surfaces are nearly flat.


*Keywords:* Polyamide 6; Deformation; Texture

## 1. Introduction

In most cases, the deformation of a semicrystalline polymer leads to an increase in material's strength and toughness. Various processes have been designed in industry to achieve permanent plastic deformation, however, permanent deformation of polymeric materials is usually obtained by simple elongation. Some disadvantages caused by the type of a processing method can often be found in final products. For example: in tensile drawing the strength becomes high in one direction but weakness appears in perpendicular directions, cavitation shows up in a drawing process due to mechanical mismatch of adjacent stacks of lamellae [1] or strap widening occurs in a simple rolling process which can result in edge cracking. Although in a compression one can avoid cavitation, the process can be hardly designed as a continuous operation. Recently, a new deformation method combining the compression and rolling was developed, which is known as rolling with side constraints [2,3]. The advantage of this method is the possibility to compress relatively thick, wide, and infinitely long rods or profiles in a continuous manner. The resulting profiles may have a considerable high cross-section and superior mechanical properties. Before utilizing this new process, it is necessary to understand the plastic deformation mechanisms of the polymer materials deformed by this method and to explore their macroscopic-mechanical behavior by taking into account the individuality of a polymer. A series of studies on high-density polyethylene (HDPE) and polypropylene (PP) had been carried out by Bartczak, Morawiec and Galeski [4–6] via this new method. In the present study, polyamide 6 is used because of its special features and industrial importance.

Some important factors should be taken into account when utilizing this new method:

(1) *Friction-induced simple shear strain, especially at the high deformation ratio*. Since the friction of the roll against the

* Corresponding author. Tel.: +48 42 680 3250; fax: +48 42 680 3261.
*E-mail address:* andgal@bilbo.cbmm.lodz.pl (A. Galeski).
[1] On leave from Institute of Materials Science, Martin Luther University Halle-Wittenberg, D-06099 Halle/Saale, Germany.

0032-3861/$ - see front matter © 2006 Elsevier Ltd. All rights reserved.
doi:10.1016/j.polymer.2006.02.061

surface of the rolled material becomes more important at high deformation ratio, the flow is stronger near the rolled surface rather than that in the center. Such differences in the local strain cause unwanted side effect that leads to premature longitudinal fracture of the bar occurring near to the rolling surface. This has been demonstrated by Bartczak, Morawiec and Galeski for the HDPE and PP [4,6].

(2) *Rear minute bugling*. As a material is capable of flow; the rear minute bugling becomes possible. When a material cannot accommodate in the constraint direction, the rear bugling maybe more intensive as compared with simple rolling.

(3) *Processing limit*. Materials can only be drawn into the nip when the horizontal component of the friction is larger or equal to the opposing horizontal component of the normal force, i.e. a maximum angle of acceptance exists. The maximum angle of acceptance limits the deformation ratio during a single step of rolling, therefore, high deformation ratio can not be achieved in a single step of rolling process. For larger deformation ratio in a single step larger radius of rolls is required.

(4) *Residual stress*. Residual stress are present at a certain low level because the material is unloaded before cooling down. In addition the toughness of PA6 leads to a substantial heating upon plastic deformation. Due to the nature of its poor thermal conductivity, the time allowed for relaxation after unloading is longer and the level of thermal-induced residual stress can be lower in comparison to other polymeric materials.

(5) *Relaxation time*. When the material is forced to deform quickly between the nips of rolls, the material is subjected to a short relaxation under load, and this leads to unwanted instabilities of deformation in the skin of the rolled plaque.

All these factors mentioned above influence the properties of the final product simultaneously. Moreover, it complicates the microscopic deformation mechanism during the processing. Consequently, direct analyses of those factors are quite complex and not trivial.

By comparing the structure and mechanical properties of final products produced by the two plane–strain deformation methods, i.e. side-constraint rolling and channel-die compression, the present study attempts to find out the effects of mentioned factors in final products and the deformation mechanisms in side-constraint rolling. The reason of choosing these two methods is their relative similarity: in both methods the dimension of the material in the constraint direction is fixed, i.e. the deformation occurs in one plane and there is no shear out of that plane. These two methods are attempted to be carried out under similar conditions for easier comparison, however, inevitably slightly different parameters are employed due to the limitation of equipments and procedures. Among these different parameters, the most important one is the time allowed for post-deformation relaxation, which is always longer for the sample compressed in a channel die. The authors believe that the results still can be comparable by taking into account the relaxation in both processing methods.

## 2. Experimental

### 2.1. Virgin material used

Polyamide 6 (Boramid 6G, Nylonbor Co., Poland) was used in this study. The 1000 mm × 1000 mm × 12 mm plates of virgin material were produced by reaction injection molding (RIM) using ε-caprolactam. The density of this material is 1.13–1.14 g/cm$^3$, crystallinity entirely in the form of α-crystals of 33–35% based on DSC melting enthalpy, the melt flow index is 4.38 g/10 min, the molecular weight $M_w$ = 53,000 g/mol as measured by size exclusion chromatography in a mixture of hexafluoropropanol and methylene chloride and moisture pick-up at saturation at 60% rhm was found to be 1.7%. The melting temperature of the virgin material is 219 °C as measured by DSC.

### 2.2. Deformation

The deformed samples were obtained by using a channel-die compression and a rolling with side constraints. The compression in a channel-die was performed by using the loading frame of 10-ton capacity (Instron, Model 5582). The desired temperature was maintained by attaching two heaters to the side of a channel die. This device is shown schematically in Fig. 1.

Some details of the device were given by Bartczak et al. [6]. The size of samples for channel die compression was 10 mm thick, 40 mm high and 50 mm wide. Before compression, all surfaces of the samples were covered with molybdenum disulfide lubricant for minimizing the friction effect. The sample and the channel die were heated up to a desired temperature. The samples were compressed with a constant rate by a plunger until reaching the desired compression ratio; the temperature of channel die was maintained during the whole process. A series of trials with varied the compression rate and temperature allowed to maximize the ultimate obtainable deformation ratio: the channel-die compression

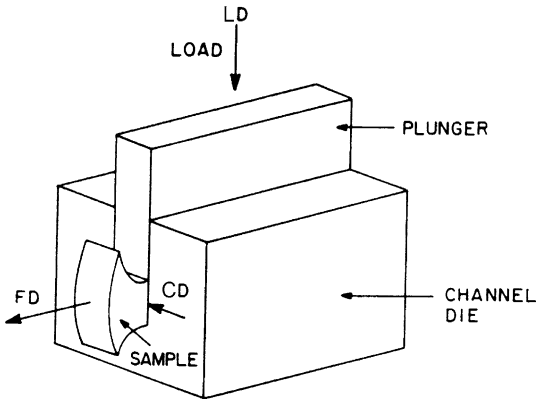


Fig. 1. Scheme of channel-die compression, defining three principal direction: free (flow) direction (FD), constraint direction (CD), and load direction (LD).

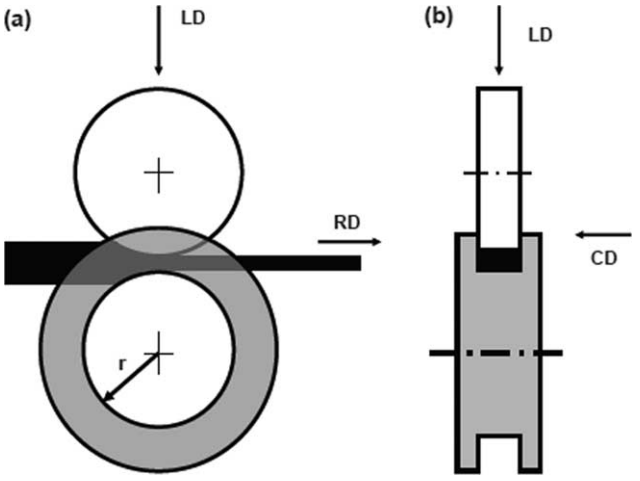


Fig. 2. Scheme side-constraint rolling (a) side view (b) front view, defining three principal direction: rolling direction (RD), constraint direction (CD), and load direction (LD).

was performed at 200 °C and loading speed of 5 mm/min. The samples were allowed to cool down to the room temperature in air, and then the load was released. For convenient later discussion, the compression ratio (CR) is defined as the ratio of the initial height to the final height of the compressed sample and three principal directions of deformation are given in Fig. 1, i.e. the load direction (LD), the flow direction (FD), and the constraint direction (CD). Rolling with side constraints was performed by a rolling apparatus constructed according to the new concept, which is presented in Fig. 2.

Some details of this device were given by Galeski, Morawiec, Bartczak and Przygoda [2,3]. Also for side constraint rolling a series of trials with varied the compression rate and temperature allowed to maximize the ultimate obtainable deformation ratio: before the start of rolling, the rolls and the raw material were heated up to 185 °C, and this temperature was maintained during the whole process. The PA6 plaques, 12 mm-thick, 1000 mm-long, 75 mm-wide were fed into the apparatus and squeezed in a channel formed between a pair of heated, driven rolls; the linear speed of rolls was 11 mm/min. The deformation ratios in the range of 1.75–3.94 were selected to explore the evolution of structure and morphology during the side-constraints rolling. Similarly, as for channel die compression, deformation ratio (DR) is defined as the ratio of the initial height to the final height of the rolled sample, and three principal directions of deformation are given in Fig. 2, i.e. the load direction (LD), the rolling direction (RD), and the constraint direction (CD).

### 2.3. WAXD

The orientation of the crystals in the deformed PA6 was studied by wide-angle X-ray diffraction measurement (WAXD). A wide-angle X-ray diffractometer system with pole figure attachment was employed. The X-ray diffractometer was controlled on-line by a computer. X-ray source was Cu $K_\alpha$ radiation generated at 30 kV and 30 mA, filtered by a thin Ni-filter and electronically. The specimens for X-ray investigation were cut from virgin material as well as from samples with different compression-ratios (CR) and deformation-ratios (DR), respectively. The cutting plane was perpendicular to FD for compressed samples, and perpendicular to RD for rolled samples. The size of each specimen was roughly 12 mm × 10 mm × 1.4 mm. The following diffraction planes for PA6 were of special interest: (200), (002) and (0 14 0) (nearly perpendicular to the molecular chain axis, see [1] and [7] for details) of α-crystallographic form at $2\theta = 20.23$, 24.00 and 77.27°, respectively, and (0 14 0) plane of γ-crystallographic form at $2\theta = 81°$ for rolled samples at DR = 3.94. The α-crystallographic unit cell parameters are: monoclinic $a = 0.956$, $c = 0.801$, $b = 1.724$ (chain axis) and $\beta = 67.5°$ while the γ-crystallographic unit cell parameters are: hexagonal $a = c = 0.48$ nm, $b = 8.6$ nm (chain axis) and $\beta = 60°$ (see Holmes et al. [8] and Gurato et al. [9]). The (0 14 0) reflections are relatively weak and cannot be easily detected in unoriented PA6, however, in highly oriented PA6 the (0 14 0) reflections from α- and γ-crystals are non-overlapping and clearly seen at $2\theta \approx 77°$ for α-crystals and at $2\theta \approx 81°$ for γ-crystals. Those reflections can be easily used for the determination of orientation of chain axes separately of α- and γ-crystals. Pole figures for the Euler angles projection of sample orientation with respect to the incident beam were obtained: the angle $\alpha$ ranged from 0 to 50° in steps of 5° in transmission mode and from 50 to 90° in steps of 5° in reflection mode; and angle $\beta$ ranged from 0 to 360° in steps of 5°. Due to significant broadening and overlapping of X-ray reflections for PA6, the diffracted intensities are often superposition intensities from several peaks and amorphous halo. Care was taken in selecting slit system to minimize the overlapping. These diffraction curves were then corrected for absorption and polarization. The pole figures were constructed based on total intensities of the peaks for all reflections of interest.

### 2.4. SAXS

The changes in lamellae structure due to deformation were studied by means of two-dimensional small angle X-ray scattering (SAXS). The X-ray beam was generated from Cu $K_\alpha$ radiation with Ni filtration at 50 kV and 40 mA,. The primary beam was collimated by a pinhole diaphragms and a capillary and the patterns were recorded on imaging plates (Eastman Kodak, Rochester, NY). The distance between a specimen and an imaging plate was 1100 mm. Air was removed by pumping from the enclosed pathway of scattered X-ray to minimize background scattering. Exposed imaging plates were read out with a PhosphorImager SI scanner (Molecular Dynamics, Sunnyvale, CA). The cutting planes of the specimens used in SAXS investigations were perpendicular to the three principal directions for both compressed and rolled samples. It enabled the views along all three principal directions. The size of all the specimens was the same as that in WAXD.

### 2.5. Tensile tests

Quasi-static mechanical properties of deformed sample were studied by means of the tensile testing machine (Instron mode 5582). The specimens for tensile test were machined from bars of rolled and compressed samples; cutting planes were parallel to FD for compressed samples and RD for rolled samples. These specimens were oar-shaped; the geometry of gauge section was $25\times4\times1$ mm$^3$. The crosshead speed of the machine was 5 mm/min, which corresponds to the initial deformation rate of 20%/min, and the distance between clamps was fixed at 40 mm.

### 2.6. SEM

Scanning electron microscope (SEM, Jeol 5500LV) was used at 20 kV to visualize the fracture surfaces obtained after the tensile tests. The fracture surface of selected samples was sputtered with ca. 10 nm gold film prior to the SEM imaging.

### 2.7. DMTA

The dynamic mechanical properties of the deformed samples were measured in a double-cantilever bending mode with a MKIII dynamic mechanical thermal analyzer (Rheometric Scientific Inc., Epson, UK). The storage modulus ($E'$) and loss factor (tan $\delta$) were registered. The specimens were machined from the deformed bar parallel to FD for compressed samples and parallel to RD for rolled samples, respectively. The geometry of every specimen was $50\times10\times$ 1.1 mm$^3$. The specimens were bent along the LD and the distance between cantilevers was fixed as 2.8 mm. The measurements were performed at a constant frequency of 1 Hz, in a temperature range from $-120$ to 200 °C and a heating rate of 2 °C/min.

### 2.8. DSC

The melting behavior of the deformed samples was characterized with a TA 2960 differential scanning calorimeter (Thermal Analysis, New Castle, DE). The heating ramp was 10 °C/min. The pieces of 6–8 mg weight were cut from the deformed samples in the plane perpendicular to three principal direction for both compressed and rolled sample. As a reference, an undeformed sample with a similar thermal history was also investigated.

## 3. Results and discussion

Channel die compression of PA6 was performed at different temperatures ranging from 150 to 210 °C with a constant compression rate from the range of 1–10 mm/min. It appeared that the highest ultimate compression ratio can be obtained at the temperature of 200 °C and the compression rate of 5 mm/min. Exemplary truestress vs. true strain curve for PA6 compressed at 200 °C with the rate of 5 mm/min in a channel-die is presented in Fig. 3.

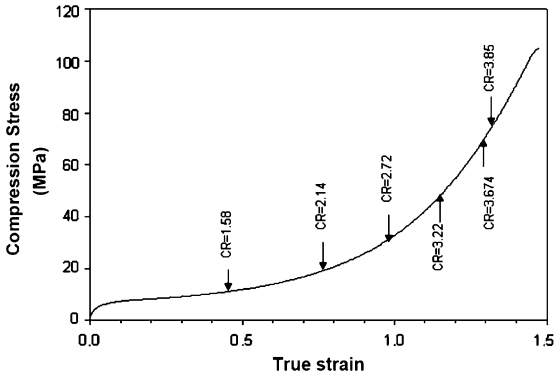


Fig. 3. Stresstrue vs. strain curve obtained for PA6 compressed with the rate of 5 mm/min in a channel-die at 200 °C. Compression ratios (CR) of samples used in the further study are marked on the curve.

It is seen that the initial rapid increase in stress is followed by plastic yielding and plastic flow. Shortly, a significant strain hardening takes place generating stresses up to 100 MPa. At the true strain of 1.45 (compression ratio of 4.26) the samples usually undergo fracture. Several PA6 samples were compressed to a desired compression ratio and then cooled down and the compressive load was released. Compression ratios (CR) of samples used in further studies are marked on the curve in Fig. 3. Samples having similar compression ratios produced by constrained rolling were also prepared for these studies.

### 3.1. WAXD

Figs. 4 and 5 show the pole figures of diffracted X-ray intensity of α-crystals in the sample deformed by channel-die compression and by side-constraint rolling, respectively. The Bragg reflection angles for (200), (0 14 0), and (002) planes were 20.23, 77.27, and 24.00° respectively. It can be seen from both Figs. 4 and 5 that the texture becomes sharper and better defined as the CR and DR are increased. The texture in the samples deformed by both methods resembles a twinned (002) α-crystals texture. The (002) plane normals are distributed very closely around the LD while (0 14 0) plane normals distribute very closely around the flow direction (FD in compression and RD in rolling). Note that the macromolecular chains in PA6 are perpendicular to the (0 14 0) planes, thus the conclusion can be drawn that macromolecular chains in deformed samples are aligned in the flow direction (FD or RD). Since the lamellar crystals of the deformed PA6 are predominantly in the α-form as it follows from the WAXS studies, these pole figures make it clear that the (002) planes containing hydrogen bonds of the textured materials are aggregated with their normals parallel to LD. As shown in (200) planes of compressed samples, one set of plane normals distributes about $+20°$ to CD direction, and the other about $-20°$ to CD direction. In the case of rolled samples, similar feature is observed, at the angles $\pm26°$. Since the projection Euler angles of $\beta$ were measured in the 5° step, i.e. the uncertainty is $\pm5°$, the plane normals distribution are approximately in the same range. Clearly, the dual orientation of the (200) planes results from the twinned position of

monoclinic PA6 crystals with fixed position of (002) planes. Similar result can be found in the references [1,10].

This situation is shown in Fig. 6.

The pole figure for (0 14 0) normals of γ-crystallographic form in rolled PA6 sample at DR = 3.94 is presented in Fig. 7. Note that hydrogen bonds in γ-form have random spatial positions around chain axes. It is quite clear from this plot that the normals to (0 14 0) planes are concentrated at around 20° with respect to the FD.

This result suggests that macromolecular chains in the γ-form crystals are oriented at some acute angle with respect to the flow direction. In contrast, macromolecular

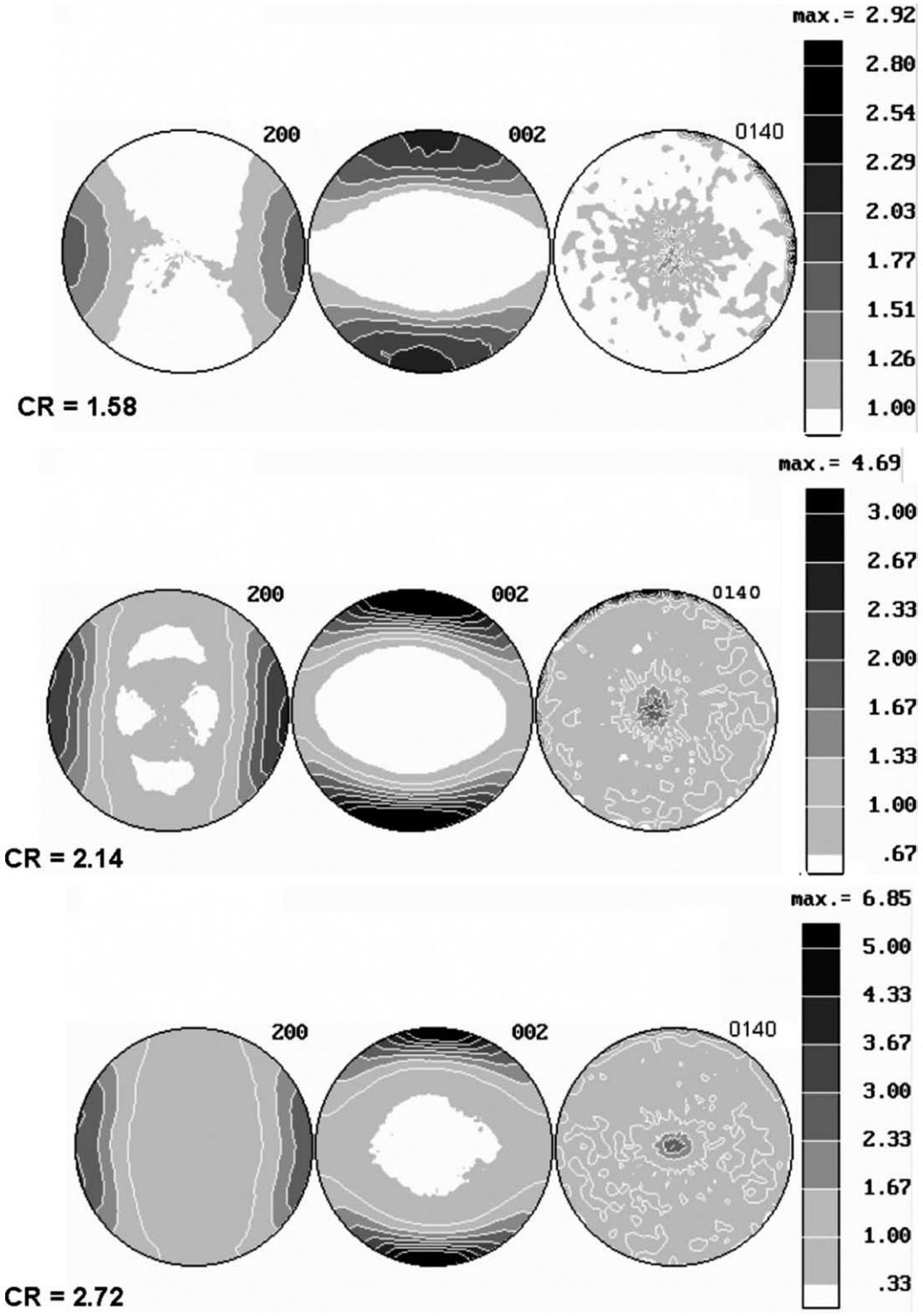


Fig. 4. Pole figures of normals to (200), (002) and (0 14 0) planes (γ-form crystal) of PA6 deformed by channel-die compression. Compression ratios (CR) are denoted.

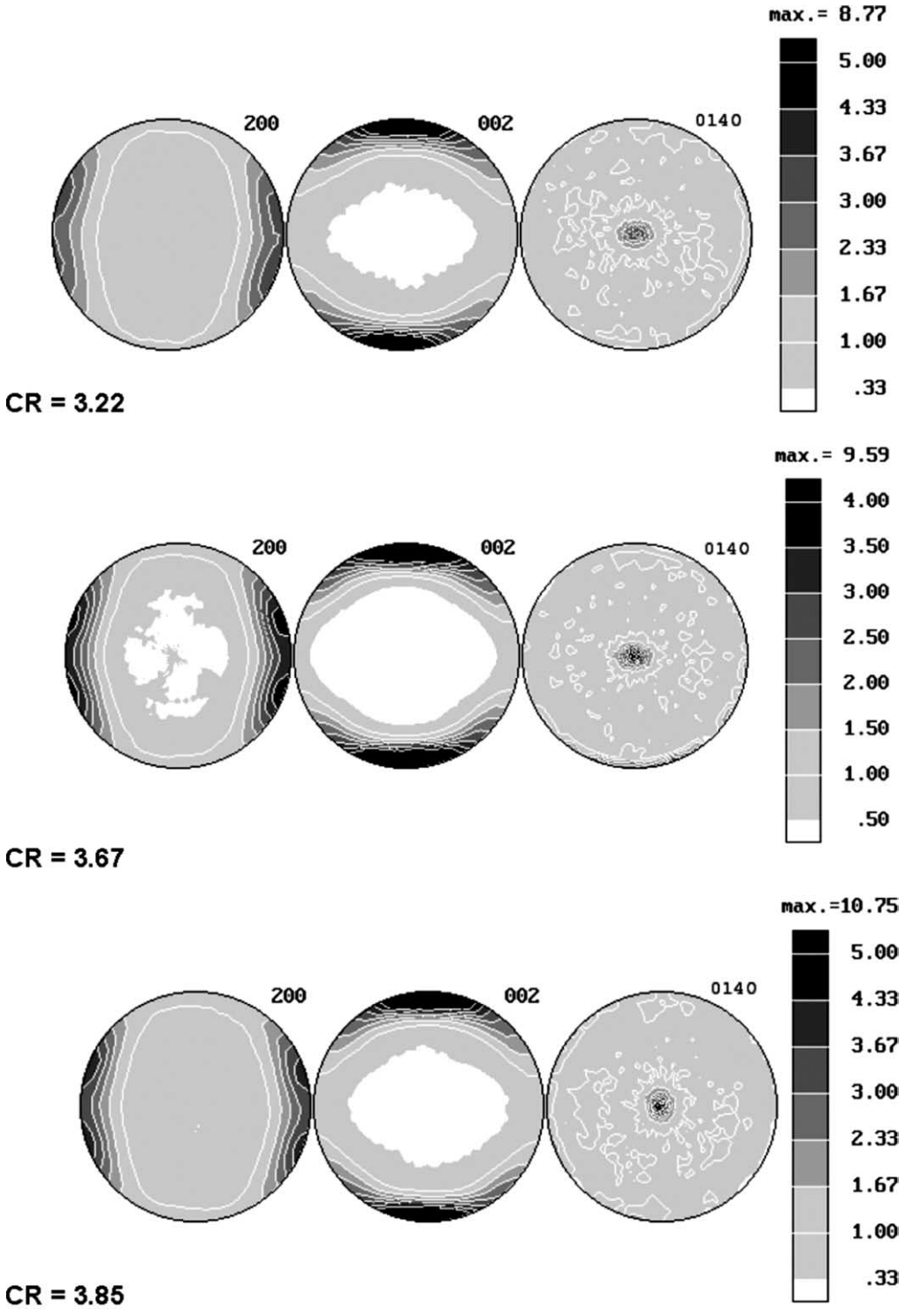


Fig. 4 (*continued*)

chains in α-form crystals are aligned along the flow direction (see the pole figure for normals to (0 14 0) planes of the α-crystals in Fig. 5). It was reported earlier by Galeski et al. [1] that shear bands arise in PA6 at the stage of CR = 1.6–1.8, at roughly ±45° with respect to the FD; at that stages of compression the α-crystals are already significantly oriented with macromolecular chains towards flow direction. Newly appeared γ-crystals are initially inclined ±45° with respect to the flow direction exactly as do the shear banding planes. The shear bands are evidenced in Fig. 8 where a polarized light micrograph of 5 μm thick section in CD view of rolled PA6 sample (DR =

3.1) is presented. Groups of dense shear bands inclined by $\pm 25^{\circ}$ with respect to FD direction are seen. Each group is roughly 20 μm in size

As DR increases to 3.94, the α-crystals are aligned nearly parallel to the flow direction while the γ-crystals are still tilted, now around 20° away from the flow direction, thus, α- and γ-crystals are misaligned at higher DR. Apparently, the alignment of PA6 γ-crystals are related to cross-hatched structure of the shear planes. The most reasonable explanation for these observations is that the shear strain acting along shear bands generates high orientation of chain fragments along shearing planes. The crystallization of those chain fragments in the form of γ-crystals that follows, preserves the orientation of the chain fragments. Further deformation causes the tilt of the macromolecular chain axes in γ-crystals towards FD.

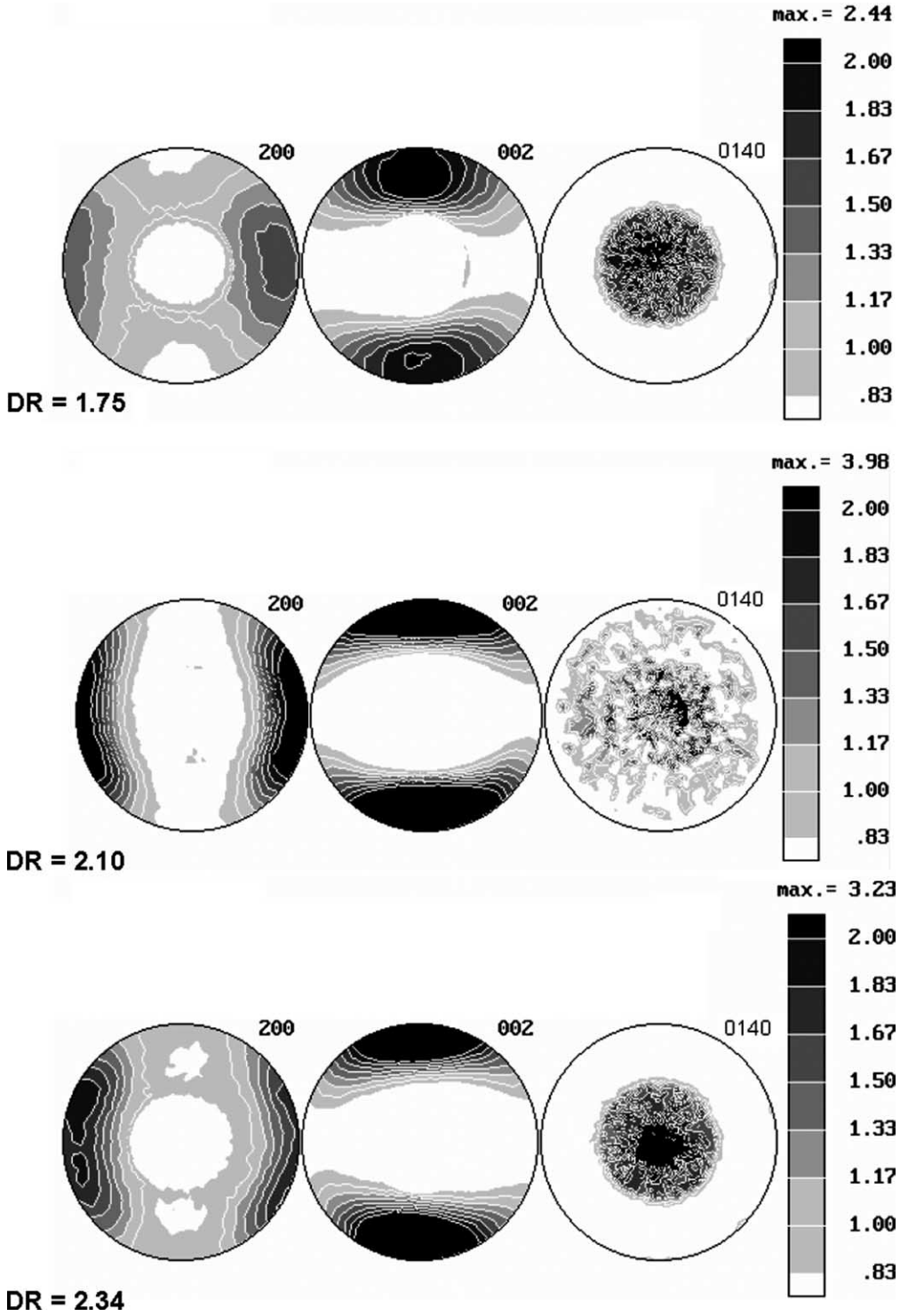


Fig. 5. Pole figure of normals to (200), (002) and (0 14 0) planes (γ-form crystal) deformed by side-constraint rolling. Compression ratios (DR) are denoted.

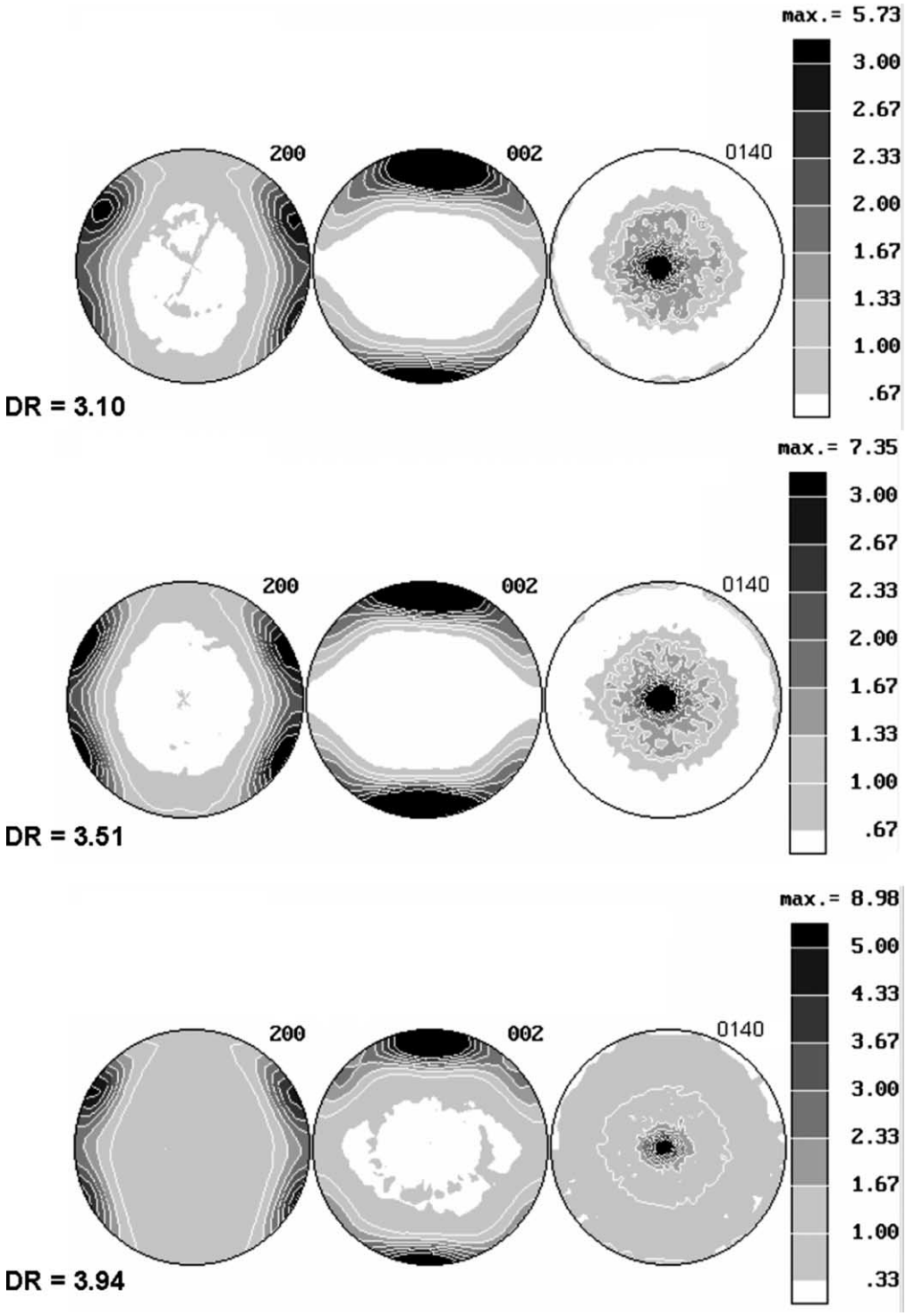


Fig. 5 (*continued*)

### 3.2. SAXS results

Figs. 9 and 10 show the SAXS patterns of textured PA6 viewed along three-principal directions for compressed and rolled samples, respectively. As a reference for both deformed samples, Fig. 11 shows the SAXS patterns of the undeformed sample. The scattering pattern of undeformed sample exhibits a well-defined isotropic ring, which reveals the presence of well developed and randomly distributed lamellae. The long period of undeformed sample as calculated from the SAXS pattern of Fig. 11 is 9.0 nm.

The SAXS patterns of deformed samples at nearly the same DR by the two methods develop in a quite similar way.

The SAXS patterns of deformed PA6 by compression alter as the DR increases (Fig. 9):

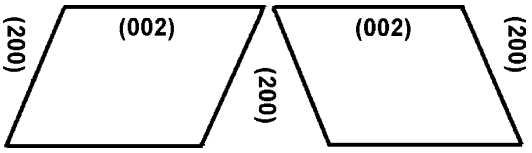


Fig. 6. Twinned positions of PA6 crystals in samples deformed by channel-die compression and side-constraint rolling.

(1) At CR = 1.58, the FD-view pattern is elliptical with the long axis along the LD, the CD-view pattern indicates peak intensity slightly shifted to $\pm 45^{\circ}$ from the LD direction; the LD view pattern shows no drastic change: the change corresponds to a decrease in long period along the LD from 9 to 8.1 nm which can be explained as a thinning induced by chain slip in crystals and interlamellar slip.
(2) As CR is increased to 2.14 the FD-view pattern shows the disappearance of the scattering, the CD-view indicates further shift of the peaks towards LD; in the LD-view pattern the peak intensity gradually shifts towards FD with long period of 9.3 nm. These alterations in SAXS pattern can be interpreted as the shear strain induced intense kinking of lamellae, which were initially oriented with their normals in the FD.
(3) As CR approaches 3.67, the LD-view pattern and the FD-view pattern show the same alteration trend as for lower CR value, while the CD-view pattern shows a shift of peak intensity, which results in a diffused four-point pattern. Such patterns indicate that the α-crystalline domains in the oriented materials can be described as chevron-shaped crystalline slabs when viewed from CD direction, with macromolecules aligned in FD [10].
(4) At CR = 3.85, the CD-view pattern shows the four-point pattern completely transforms into a very broad two-point pattern. The alteration of the CD-view pattern at the stage from CR = 3.67 to 3.85 indicates lamellae fragmentation and the emergence of a new long period along FD of 6.5 nm.

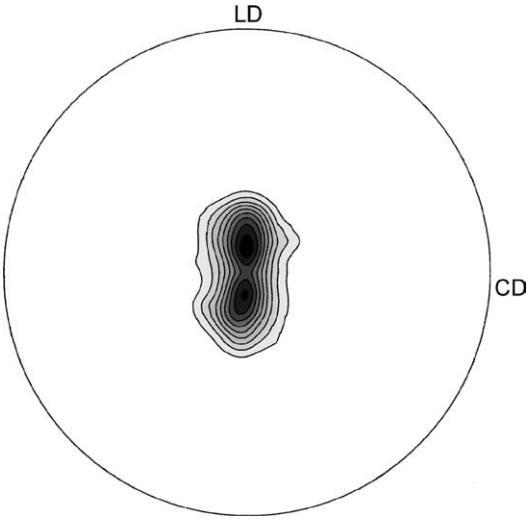


Fig. 7. Pole figure in stereographic projection for (0 14 0) normals of γ-crystallographic form in rolled sample at DR = 3.94. The net of angles are plotted every 5° for vertical and azimuthal angles. The X-ray data were collected at $2\theta = 81^{\circ}$, slit system same as for the pole figures presented in Figs. 4 and 5.

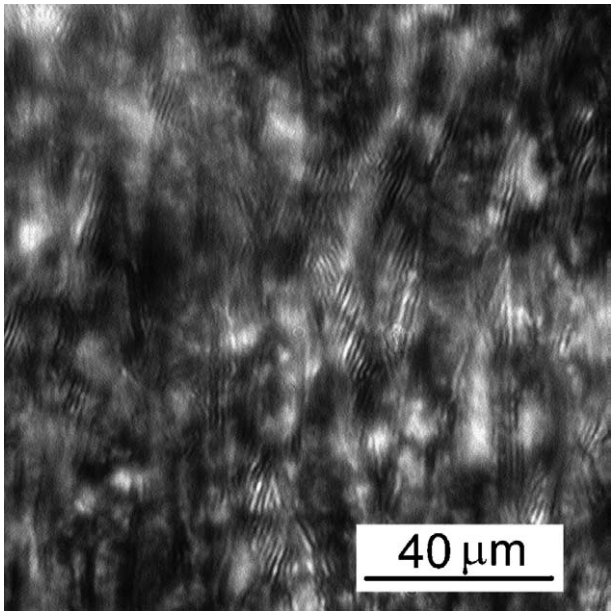


Fig. 8. Polarized light micrograph of a 5 μm thick section of PA6 sample rolled with side constraints to the DR = 3.1 at 185 °C with the rolling rate of 11 mm/min. CD view.

In summary, such alteration of lamellar crystals can be deduced from such scenario: initial deformation of lamellae during compression consists primarily of intense crystallographic chain slip in lamellae and interlamellar slip, these lead to a thinning of both amorphous layers and lamellae, and also causes a rotation of lamellae normals towards the LD direction. Following this alteration, lamellae fragmentation and the emergence of a new long period along the FD (or RD) direction take place at higher compression ratios. The crystallite fragments associated with the new long period have a much smaller dimension along the LD direction (6.7 nm) than the length of the lamellae in the spherulites. A similar scenario was proposed earlier by Galeski et al. in HDPE [11], although the changes may take place at different CR due to individuality of that material. This is in contrast to earlier observation of the formation of a new long period in tensile drawing [12,13]. In tensile drawing the fragmentation of lamellae occurs at yielding and it is associated with cavitation. The formation of a new long period in that case was explained as simultaneous processes of melting and recrystallization under adiabatic conditions[14,15]. However, in compression such phenomena like micronecking, lamellar fragmentation and voiding processes are avoided up to the compression ratio far above the yield point and crystallographic mechanisms of plastic deformation are engaged. No melting-recrystallization is observed in plane–strain compression. The new long period in plane strain compression is the effect of a series of phenomena; continuing monotonic shearing and thinning of lamellae become unstable—much like thinning and cappilary breakdown of layered fluid—and responds by periodic fragmentation of lamellae The respective thermodynamic

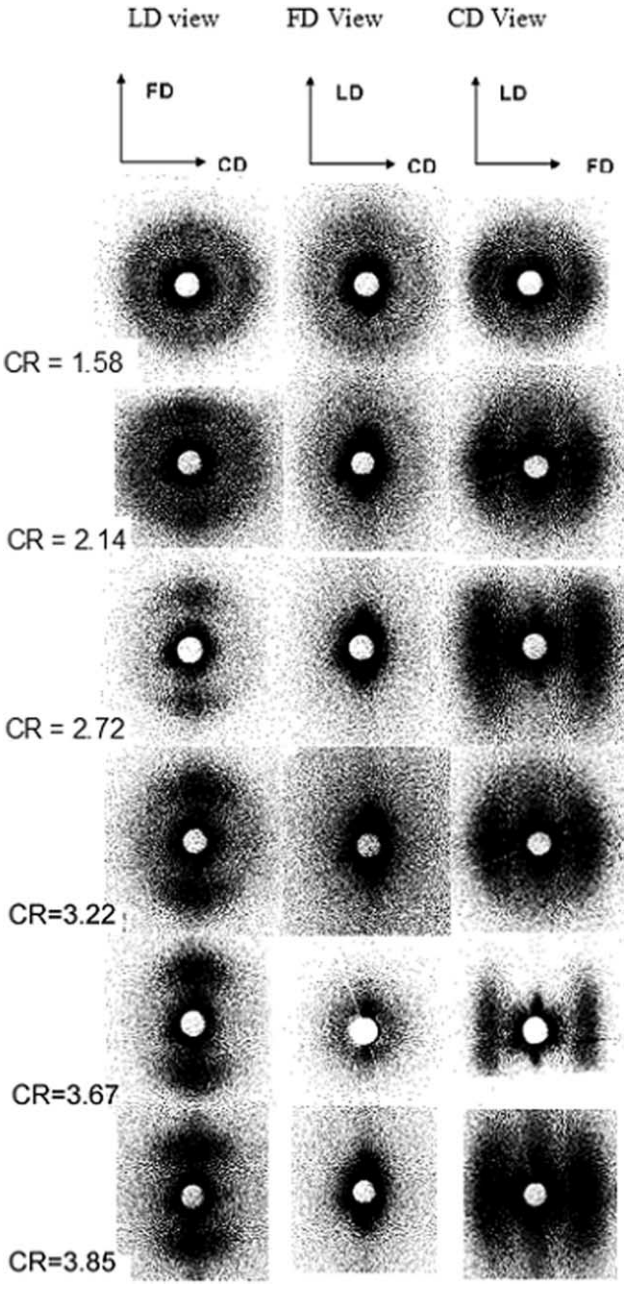


Fig. 9. SAXS patterns of PA6 deformed by channel-die compression. Views from three perpendicular directions LD, FD and CD.

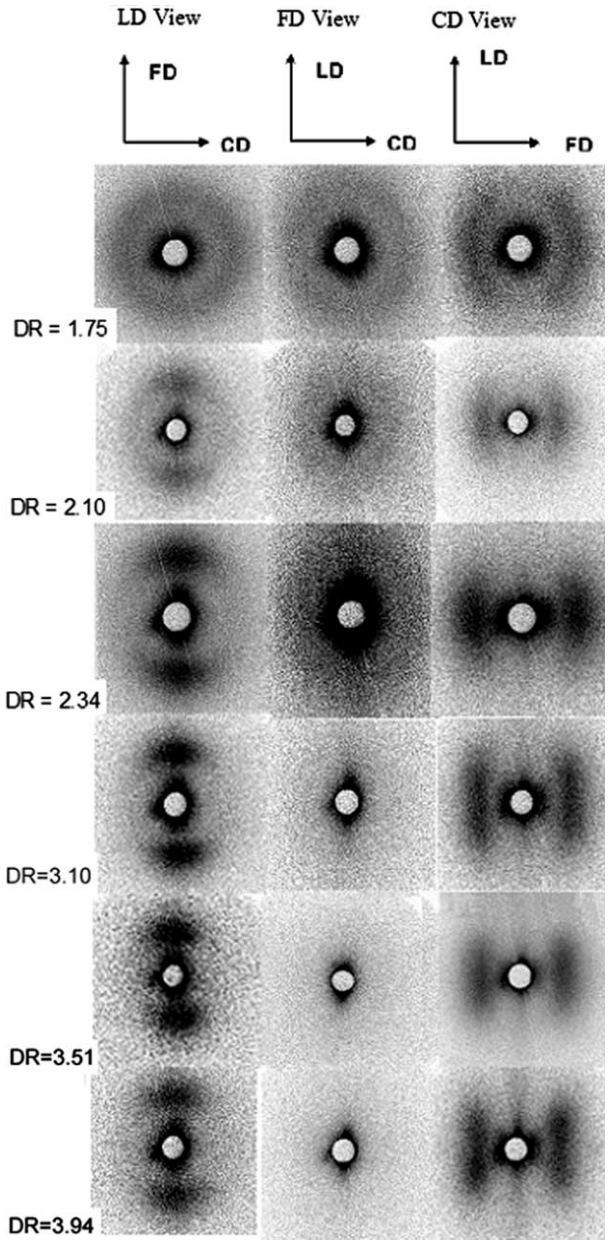


Fig. 10. SAXS patterns of PA6 deformed by side-constraint rolling. Views from three perpendicular directions LD, FD and CD.

consideration for the conditions of lamellae fragmentation was presented earlier in Ref. [11]. Once the lamellae are fragmented, the fragments have now more freedom and can change shape and orientation to reduce the interfacial energy. This should happen by the migration along the chains of the accumulated defects. This purely topological reordering give rise to a new long period where the new topologically reordered lamellar fragments touch and slightly associate. It must be noticed that the new long period, which appear in plane strain compression, is much less pronounced than the new long period formed during tensile drawing. In fact in the paper by Schoenherr, Vancso and Argon [16] concerning the AFM studies of channel die compressed HDPE deformed to the compression ratio of 6.44 (the sample from the work of Galeski et al. [11]), the molecular resolution in AFM images was achieved. Molecular resolution reached in their studies revealed no clearly identifiable amorphous layers over several expected long period dimensions, confirming the dispersion of the amorphous material and the diffusion of previously clear amorphous–crystalline interface. Although the pole figures and SAXS patterns of the specimens prepared by these two methods look quite similar, they still show some differences if examined in details (1) comparing the pole figures: the rolled samples exhibit less sharp texture than the compressed ones at similar values of DR and CR (2) comparing SAXS patterns: four-point pattern is distinct at CR = 3.67 in compressed sample, but not found in the rolled sample with similar DR; in addition, the appearance of diffused two-point pattern is at

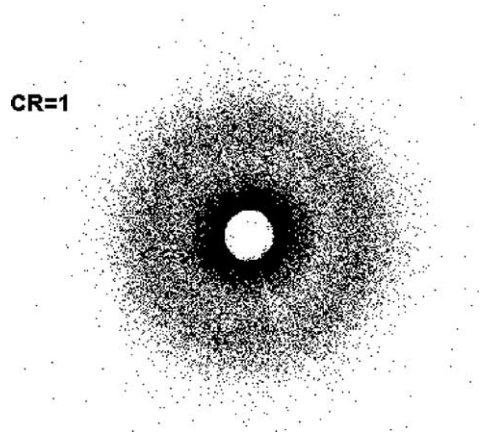


Fig. 11. SAXS patterns of undeformed PA6.

DR = 3.10 for a rolled sample, much earlier (Fig. 10) than for a compressed sample.

All these imply that the fragmentation of lamellae takes place in rolling earlier than in channel die compression. It is seen from the true stresstrue strain curve in Fig. 3 that the CR values at which lamellae fragmentation takes place corresponds to the onset of intensive strain-hardening. This observation suggests that the hardening stage is the starting point of the divergence of morphology produced by these two methods.

The reasonable explanation for such difference is the time allowed for creep during compressive load by both methods. At the hardening stage, crystals have already undergone severe slips and the amorphous phase is strongly extended, i.e. the amorphous phase exhaust the ability of accommodating the shape changes of crystals. In channel-die compression, the highly deformed sample for significantly longer time before its cooling and removal of load. Hence the retraction when the load is removed is much lower, first, because the temperature was decreased and much of the possibility of retraction was freezed and second, because the creep under load is much more advanced since the sample resides under load for longer time. In side-constraint rolling a sample flees quickly from the nip, a sample is unloaded and undergoes stronger retraction. Indeed, the entanglement network is far more extended in a compressed sample than in rolled samples at this stage as it can be judged from the onset of strain hardening and the ability of constrained rolled samples to deform more in tensile tests. Therefore, the difference in the time allowed for creep between these two methods leads to the structure and morphology differences.

### 3.3. Tensile test results

Figs. 12 and 13 show the stress–strain curves of the specimens cut out from the rods deformed by channel-die compression and side-constraint rolling, respectively. All the specimens were tested in tension along the direction of molecular orientation (i.e. FD for compressed samples or RD for rolled samples). It can be seen from Figs.12 and 13 that the stress–strain curves of both types of samples have the same trend: as CR and DR increase the curves become steeper

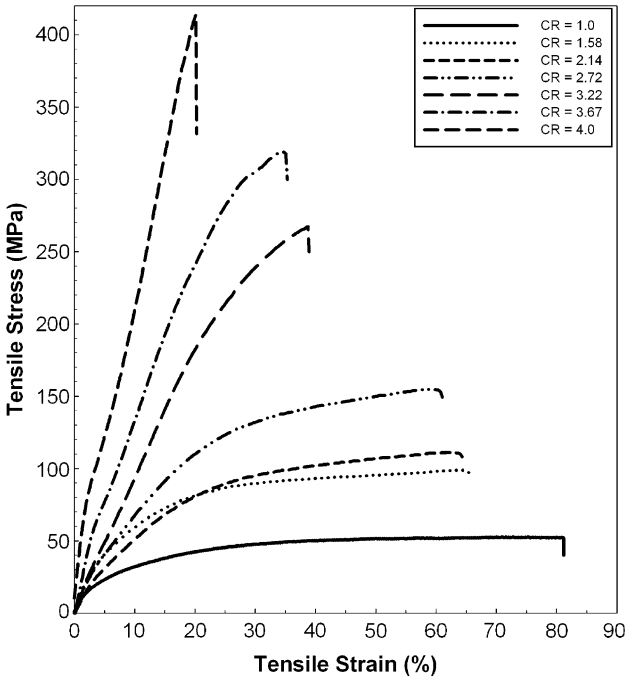


Fig. 12. Tensile stress–strain curves of compressed PA6 in channel-die compression, samples were machined to oar-shaped tensile bars in a plane parallel to FD.

reaching to the higher values of stress. The stress values at break depend on the way in which the samples were oriented: for compressed sample, when CR = 4.0, the ultimate strength is above 410 MPa at the strain of 18%; for rolled sample, at a similar DR, the strength is only 205 MPa at the strain of more than 32%, i.e. half of the strength and twice the strain obtained by channel-die compression. For comparison, it is worth to note that a low carbon steel has the tensile strength of 220 MPa. It can also be seen that the values of strain at break is always higher for rolled samples than for compressed samples. Apparently, the rolled sample is able to accommodate more deformation. SAXS results were also indicating a lower orientation of rolled samples.

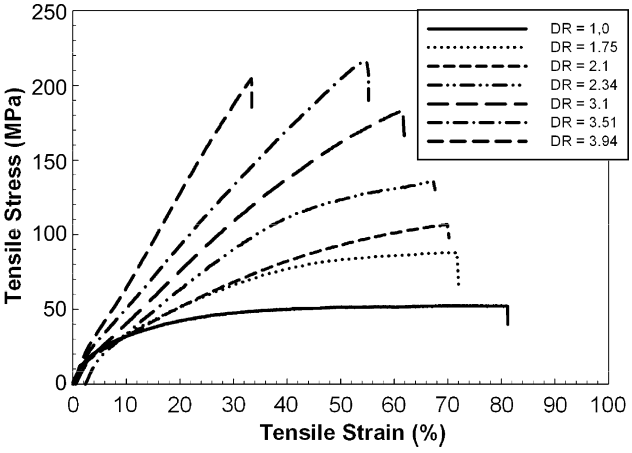


Fig. 13. Tensile stress–strain curves of PA6, deformed by side-constraints rolling, samples were machined to oar-shaped tensile bars in a plane parallel to RD.

It is very clear from the comparison of Figs. 12 and 13 that when the deformation ratio reaches 2.7, the ultimate-stresses for the two sets of samples start to diverge. Note that the CR = 2.7 is just the starting point of strain hardening during compression (refer to Fig. 3). As already shown in the SAXS results, the morphology difference between the samples deformed by the two methods becomes significant at the strain hardening stage, therefore, structure difference directly leads to the large difference in mechanical properties.

### 3.4. SEM

A very interesting feature was found in the rolled samples at DR = 3.94 via SEM. First, the fracture in tensile tests of oriented bars occurs along regular relatively smooth planes, tilted at an acute angle around 20–26° with respect to the RD (Fig. 14(a)).

It should not be incidental that the fracture planes are tilted at a similar angle as the shear bands and chain fragments in γ-crystals with respect to the RD (refer to Fig. 7). Second, some regular horizontal lines are distributed rather uniformly on these fractured surfaces (Fig. 14(b) and (c)). The average distance between those lines is in the range of 100 and 200 μm. All these evidences suggest that cracking start from the shearing zones containing γ-crystals and develop along the shear planes. As the fracture advances along a shearing plane, it encounters others crossing shear bands on its path every 100–200 μm, the fracture propagates preferring the direction of a shear band until the next shearing plane. Again, fracture advances along the new shearing plane until an encounter of a next shear band. Such propagation continues until fracture of the material. The authors propose that the bifurcation of orientation of α-and γ-crystals is the origin of this peculiar fracture behavior of rolled PA6.

Since SAXS patterns for samples deformed by side-constraint rolling and channel die are very similar (Figs. 9 and 10) and also the shear banding is similar, as presented in Fig. 8 for channel die compressed PA6, one can expect that the main deformation mechanisms, which occur in the channel-die compression, should also be valid in side-constraint rolling. The features of textured crystal structure deformed by both methods are shown in Fig. 15. Unlike polyethylene, it is imposible to obtain so-called quasi-single crystal texture for PA6 due to the nature of monoclinic structure of PA6 crystals-crystallographically dual-oriented material of orthotropic symmetry is produced in channel die compression and in rolling with side constraints. This is shown in the bottom of Fig. 15. The shear bands are produced in stacks from 8 to 10 bands in a stack and the spaces between individual shear bands are filled with α-crystalline material having the prevailing orientation along FD direction. Along the shear bands which are tilted ±25° from the FD direction for the sample compressed to CR = 3.1, the γ-crystals are aligned. The shear bands stacks are approx. 10–20 μm thick and the distances between individual shear bands are from 1 to 2 μm. When the deformation is increased to CR = 4.0 a significant fraction of shear bands cannot be recognized anymore as it can be judged from polarized micrographs of thin sections (not shown here). Also they do not manifest themselves in SEM micrographs of fracture surfaces (Fig. 14), only very few, every 100–200 μm shear bands are recognizable. However, the pole figure of (0 14 0) normals of γ-crystals (Fig. 7) clearly indicated the existence

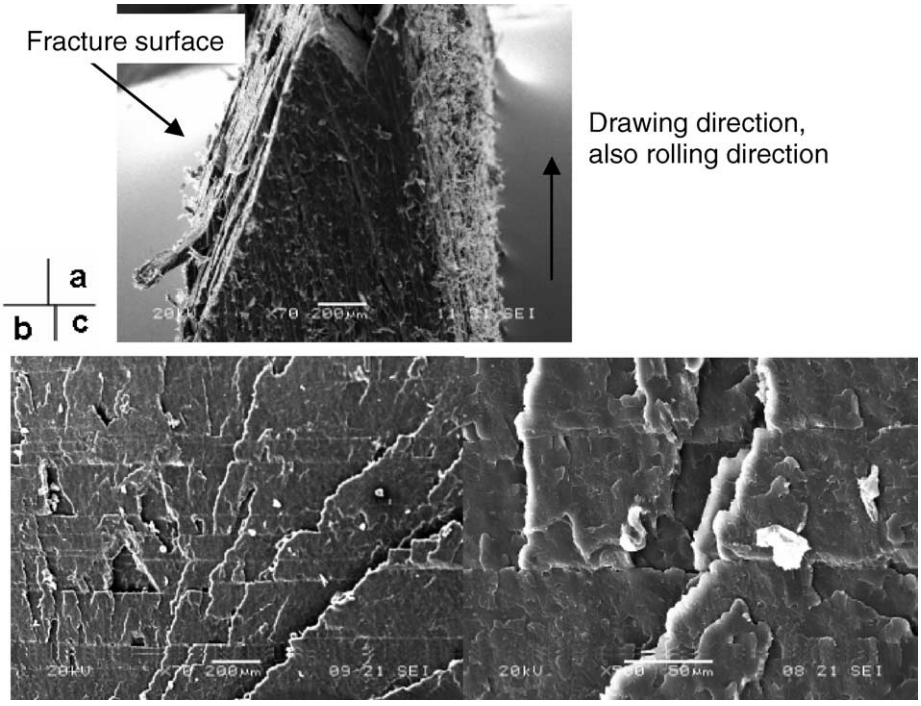


Fig. 14. Fractured surface observed by SEM, specimen was deformed by side-constraint rolling at DR = 3.94. (a) Side view shows a regular fracture at an acute angle of 26° (b) fractured surface shows some regular horizontal lines (c) magnified fractured surface of (b).

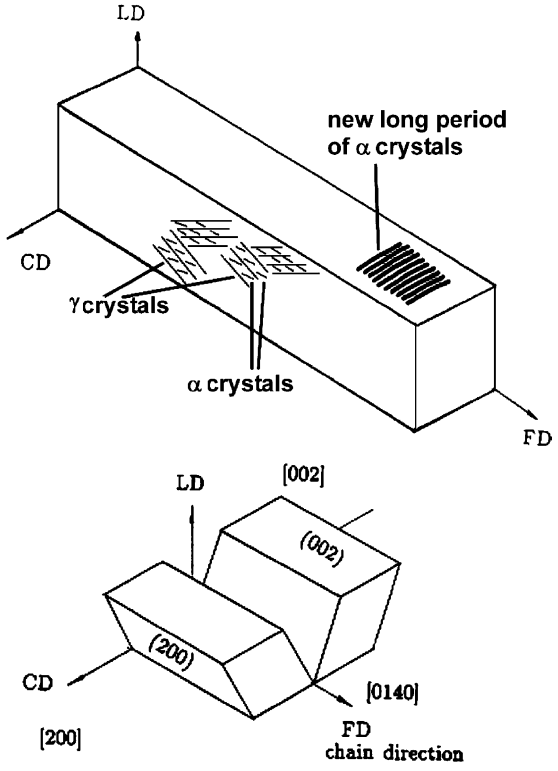


Fig. 15. Schematic orientation of the lattice and lamellar crystal of the textured PA6.

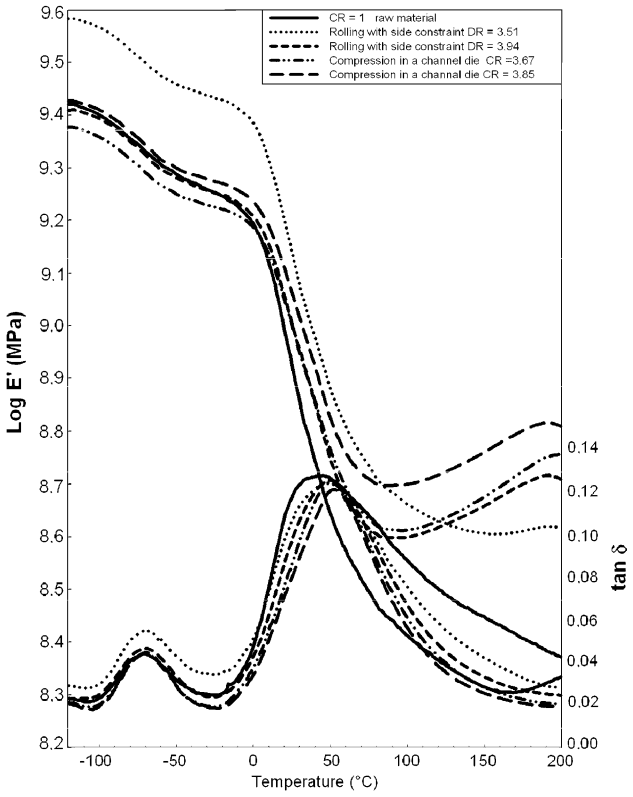


Fig. 16. DMTA curves determined in a double-cantilever bending mode at a frequency of 1 Hz and at a heating rate of 2 °C/min for samples of PA6 undeformed and deformed at CR = 3.85; DR = 3.94: $E'$ and tan $\delta$. Cutting plane is perpendicular to FD and RD.

of a fraction of γ-crystals tilted by $\pm 20^{\circ}$ from the FD direction. All these feature of highly compressed PA6 sample are shown in Fig. 15.

### 3.5. DMTA

Fig. 16 shows the DMTA curves for compressed and rolled samples. Three relaxation processes are revealed: γ-relaxation (below −110 °C, here only part of γ-relaxation peak is seen.), β-relaxation (around −70 °C) and $\alpha'$-relaxation (40 °C). It is generally accepted that the γ-relaxation involves a cooperative motion of the methylene groups between amide linkages, while β and $\alpha'$ relaxation involve motions of non-hydrogen-bonded and hydrogen-bonded amide groups in the amorphous region, respectively [17,18]. Here, the discussion is restricted to β and $\alpha'$ relaxations.

As it is seen in Fig. 16, the position of β peak is unaffected by the orientation, whereas its intensity increases. The increase in the intensity of β peak indicate the increase in the number of unbonded amide groups, the result is most likely due to internal strain produced by the plastic deformation [18]. For the $\alpha'$ relaxation peak, the orientation produces a shift of about 20 °C to higher temperatures in both compressed and rolled samples and reduces its intensity, which is clearly seen in Fig. 16. These data indicate that the orientation leads to a general tightening of the structure, which is probably accompanied by an increase in the density of the amorphous phase (see Ref. [1] for the data on amorphous phase density in channel die compressed PA6). As the material becomes highly oriented, the free volume in the amorphous phase is greatly reduced and the movements of macromolecular chains are restricted, more energy is required to activate α-relaxation, hence the $\alpha'$ relaxation peak shifts to a higher temperature. As it is deduced from the heat of melting (see below) the crystallinity degree is increasing (heat of melting is increasing from 74 to 120–130 J/g for deformation ratio of 1.6–1.8 and then the subsequent small increase in the $T_m$ and $\Delta H_m$ can be ascribed to a partial destruction of crystals due to an intense shear bands and recrystallization in the γ-form crystals). After reaching the deformation ratio of 2.8, the behavior of the rolled and compressed samples starts to diverge. For channel die compressed samples the meltinh enthalpy is continuously increasing, while this does not occur in the rolling process. The above observation indicates that some recrystallization takes place in samples compressed to high compression ratio in a channel die while in rolled samples the short duration of creep under load is not facilitating the recrystallization.

### 3.6. Melting behavior

It was noticed that the shapes of melting peaks are different when the sample was cut along CD, FD or LD. The variations of thermal signal are due to the difference in inhibition of the shrinkage and thickening connected with relaxation of orientation of highly deformed samples in the enclosures of DSC capsules. The variations are resulting from the change of

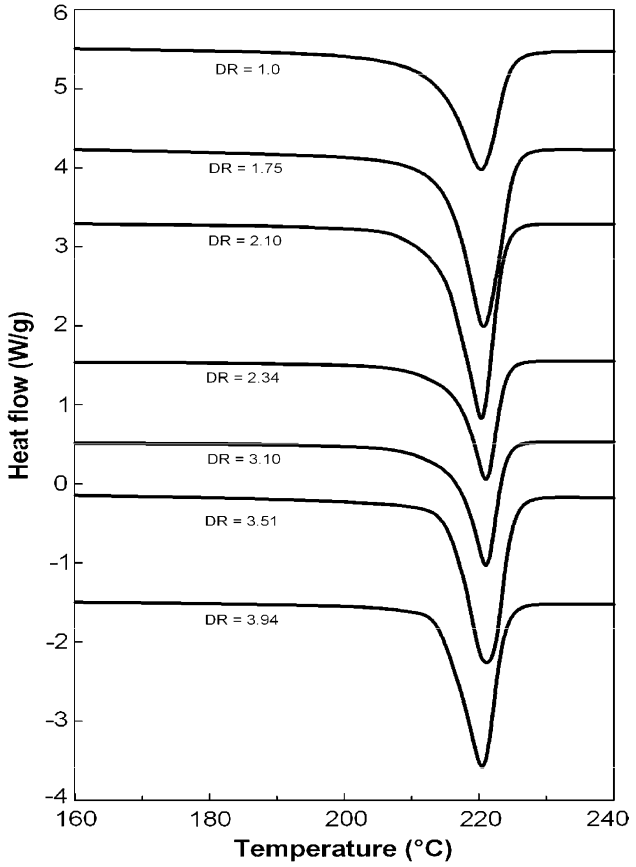


Fig. 17. Melting curves of the rolled samples, determined by DSC in a heating scan at a ramp of 10 °C/min. Cutting planes are perpendicular to LD.

thermal contacts between the shrinking sample and the DSC pan during the heating scan. The most affected by shrinkage are the highly oriented samples cut perpendicular to CD: even a double melting peak can be observed. Fig. 17 shows the DSC curves for rolled samples re cut perpendicular to LD; for that direction the smallest variations of the DSC signals connected with the sample shrinkage and thickening were observed.

Both the peak melting temperature ($T_m$) and the heat of melting ($\Delta H_m$) for both compressed and rolled samples increase with increasing DR and CR. The melting temperature is increasing only slightly from 219 to 223 °C with increasing DR or CR. The heat of melting increases from 74 to 120–130 J/g for CR or DR of 1.6–1.8 and it remains at a high level for higher deformations for both compressed and rolled samples.

The initial increase in $T_m$ and $\Delta H_m$ is closely related to the early quasi-homogeneous deformation response of the sample under increasing compression; the initial compression causes some further crystallization of the samples (see for example [1]), whereas the subsequent small increase in the $T_m$ and $\Delta H_m$ can be ascribed to a partial destruction of crystals due to an intense shear bands and recrystallization in the γ-form crystals which appear at DR and CR larger than 1.8. After reaching DR = 2.8, the behavior of the two sets of samples starts to diverge. For channel die compressed samples, $T_m$ and $\Delta H_m$ are continuously increasing, which indicates the continuation of the process of reconstruction of the disrupted crystallites. However, this does not occur in the rolling process due to a fast recovery upon unloading when the rolled bar exits quickly from the nip.

## 4. Conclusions

Two plane–strain deformation methods, i.e. channel-die compression and side-constraint rolling, have been studied in details for PA6 material. The experimental work was designed to find out the similarity and dissimilarity in structure and mechanical properties of materials deformed under these two methods. It is shown that side-constraint rolling leads to a strong orientation of crystalline component comparable to that obtained in a channel-die compression. Also, as it was shown in the past by pole figures of the X-ray diffraction integral intensity of the amorphous hallo, the high orientation of the amorphous phase of PA6 subjected to channel die compression is developed in the direction FD [1]. Similar observation of frozen-in high orienation of the amorphous phase was made for channel die compressed HDPE [11]. The course of deformation is as follows: at initial small deformation ratio the amorphous material responds independently and it is able to recover completely upon unloading, however, at higher deformation ratio the amorphous material is no longer responding independently and is forced to go along with shearing and thinning of lamellae. The recovery of the amorphous material is then strongly limited by deformed and displaced crystals and its orientation is frozen in the textured material. One of the apparent signs of the orientation of the amorphous material is a large increase in the modulus of elasticity. It is found that the crystalline texture and lamellar structure of PA6 samples after the deformation by the two mentioned methods are analogous at the corresponding strains. Pole figures analysis shows: the molecular chains in α-crystals are highly aligned in the flow direction; the (002) plane normals are distributed quite closely around the load direction; and the (200) plane normals are equally divided and oriented in the direction from ±20 to ± 26° away from the CD, resembling a twinned lattice structure. The γ-form crystals appear in both types of samples simultaneously with a massive generation of shear bands at CR and DR = 1.8 and above. The γ-form crystal texture component exhibits a cross-hatched structure as resulting from the shear bands with macromolecular chains aligned at acute angles to the texture axis of the α-crystals. The SAXS patterns show that the α-crystalline domains in those oriented materials can be described as chevron shaped crystalline slabs when viewed from CD direction, with macromolecules aligned in FD (similar feature was observed in the past, see for example [10]).

Oriented PA6 bars obtained by both methods still shows some subtle dissimilarity: α-crystals in rolled samples at high DR are oriented with their macromolecular axes parallel to the flow direction while γ-crystals are tilted away by approx. 20° with respect to α-crystal orientation. This results from shear bands, which are separated from each other by 100–200 μm. SAXS results implied that the fragmentation of lamellae takes place in rolling earlier than that in compression. It is suggested that the hardening stage is the starting point of divergence of

morphologies between rolled and compressed samples. The time allowed for relaxation under load plays an important role at this stage.

It is demonstrated that both rolled and compressed samples show a significant increase in the tensile strength. The ultimate tensile strength of rolled samples is lower than that for the compressed ones at a corresponding strain. For the compressed PA6, the tensile strength approaches 420 MPa. The rolled sample at a similar DR shows the strength of only 205 MPa and is able to accommodate more strain than the channel die compressed sample. The difference in time allowed for creep under loading in both deformation methods is responsible for those dissimilarities and this effect cannot be neglected when deformation reaches the hardening stage.

The fracture behavior of highly oriented PA6 bars shows a unique tilted flat and nearly smooth surfaces. This behavior is connected with shear bands that were generated earlier at the CR around 1.6–1.8 and above. Bifurcation of orientation of $\alpha$- and $\gamma$-crystals is the origin of this peculiar fracture behavior of rolled PA6.

## Acknowledgements

The authors would like to thank Dr J. Morawiec for his assistance in the preparation of samples via rolling apparatus, Dr Z. Bartczak for his valuable discussion and assistance with tensile test experiments, Dr T. Kazmierczak for his assistance with SEM equipment and Ms K. Gadzinowska for her assistance with DSC experiments. Mr E. Lezak for assistance with SAXS, WAXD measurements and compression test, Mr R. Masirek and Mr Z. Kulinski for their assistance with DMTA experiments. X.C. acknowledges the Martin Luther University in Halle-Wittenberg for financial support during her stay in Lodz, Poland. State Committee for Scientific Research, Poland is acknowledged for supporting this research through the grant KBN 4 T08E 055 22. The work was accomplished in the frame of IUPAC subcommittee 'Structure and Properties of Commercial Polymers'.

## References

[1] Galeski A, Argon AS, Cohen RE. Morphology of bulk nylon 6 subjected to plane–strain compression. Macromolecules 1991;24:3953.
[2] Galeski A, Morawiec J, Bartczak Z, Przygoda M. Polish Patent 178058; 2000.
[3] Morawiec J, Bartczak Z, Kazmierczak T, Galeski A. Rolling of polymeric materials with side constraints. J Mater Sci Eng 2001;A317:21–7.
[4] Bartczak Z. Deformation of HDPE produced by rolling with side constraints. Part I. Orientation behavior. J Appl Polym Sci 2002;86: 1396–404.
[5] Bartczak Z, Morawiec J, Galeski A. Deformation of HDPE produced by rolling with side constraints. Part II. Mechanical properties of oriented bars. J Appl Polym Sci 2002;86:1405–12.
[6] Bartczak Z. Influence of molecular parameters on high-strain deformation of polyethylene in the plane–strain compression. Part II. Recovery behavior. Polymer 2005;46:10339–54.
[7] International tables for X-ray crystallography, III Kynoch Press, 1962, p. 295.
[8] Holmes DR, Bunn CW, Smith DJ. The crystal structure of polycaproamide: nylon 6. J Polym Sci 1955;17:159–77.
[9] Gurato G, Fichera A, Grandi FZ, Zanetti R, Canal P. Crystallinity and polymorphism of 6-polyamide. Makromol Chem 1974;175:953–75.
[10] Lin L, Argon AS. Deformation resistance in oriented nylon 6. Macromolecules 1992;25:4011–24.
[11] Galeski A, Bartczak Z, Argon AS, Cohen RS. Morphological alterations during texture producing plane–strain compression of high density polyethylene. Macromolecules 1992;25:5707.
[12] Peterlin A. In: Baer E, editor. Polymeric materials. Metals park, OH: American Society for Metals; 1975. p. 175.
[13] Peterlin A. Molecular model of drawing of polyethylene and polypropylene. J Mater Sci 1971;6:490–508.
[14] Flory PJ, Yoon DY. Molecular morphology in semicrystalline polymers. Nature 1978;272:226–9.
[15] Gent AN, Madan S. Plastic yielding of partially crystalline polymers. J Polym Sci, Polym Phys Ed 1989;27:1529–42.
[16] Schoenherr H, Vancso GJ, Argon AS. The structure of highly textured quasi- single-crystalline high-density polyethylene probed by atomic force microscopy and small-angle X-ray scattering. Polymer 1995;36: 2115–21.
[17] Willbourn AH. The glass transition in polymers with the $(CH^{\wedge})n$ group. Trans Faraday Soc 1958;54:717.
[18] McCrum NG, Read BE, Williams G. Anelastic and dielectric effects in polymer solid. New York: Wiley; 1967.